Research Article | Vol. 30, No. 11 / 23 May 2022 / Optics Express 19573
Optics EXPRESS

Magnetically sensitive fiber probe with nitrogen-vacancy center nanodiamonds integrated in a suspended core

ADAM FILIPKOWSKI,[1,2,5] MARIUSZ MRÓZEK,[3,5] GRZEGORZ STĘPNIEWSKI,[1,2] MACIEJ GŁOWACKI,[4] DARIUSZ PYSZ,[2] WOJCIECH GAWLIK,[3] RYSZARD BUCZYŃSKI,[1,2] MARIUSZ KLIMCZAK,[1,*] AND ADAM WOJCIECHOWSKI[3]

[1]*Faculty of Physics, University of Warsaw, Pasteura 5, Warsaw, 02-093, Poland*
[2]*Łukasiewicz Research Network – Institute of Microelectronics and Photonics, Al. Lotników 32/46, Warsaw, 02-668, Poland*
[3]*Institute of Physics, Jagiellonian University in Kraków, Łojasiewicza 11, Kraków, 30-348, Poland*
[4]*Faculty of Electronics, Telecommunications and Informatics, Gdańsk University of Technology, Narutowicza 11/12, Gdańsk, 80-233, Poland*
[5]*These authors contributed equally*
[*]*mariusz.klimczak@fuw.edu.pl*

Abstract: Efficient collection of photoluminescence arising from spin dynamics of nitrogen vacancy (NV) centers in diamond is important for practical applications involving precise magnetic field or temperature mapping. These goals may be realized by the integration of nanodiamond particles with optical fibers and volumetric doping of the particles alongside the fiber core. That approach combines the advantages of robust axial fixation of NV diamonds with a direct spatial overlap of their fluorescence with the guided mode of the fiber. We developed a suspended core silicate glass fiber with 750 nm-diameter nanodiamonds located centrally in the 1.5 µm-core cross-section along its axis. The developed fiber probe was tested for its magnetic sensing performance in optically detected magnetic resonance measurements using a 24 cm-long fiber sample, with the NV excitation and fluorescence collection from the far ends of the sample and yielding optical readout contrast of 7% resulting in 0.5 µT·Hz$^{-1/2}$ magnetic field sensitivity, two orders of magnitude better than in earlier designs. Thanks to its improved fluorescence confinement, the developed probe could find application in magnetic sensing over extended fiber length, magnetic field mapping or gradiometry.

1. Introduction

Optical sensing of magnetic fields can be efficiently realized by exploiting the electron spin dynamics of negatively charged nitrogen-vacancy centers (NV^-) under resonant microwave excitation [1]. In addition to the basic principle of a magnetic-field sensor with a bulk NV-diamond placed in a localized instrument, numerous approaches are developed for remote sensing with optical fibers. Most successful designs utilize ensembles of nano-diamonds [2–4], a single miniature diamond crystal [5–10] or a single nano-diamond [11–13] attached to the fiber end. Alternative approaches to remote sensing utilize many nanodiamonds distributed in various ways along optical fibers [14–20].

Nanodiamonds offer important advantages over bulk diamonds: one being the longer fluorescence lifetime of the NV^- [21] and the second, most important in the context of this work, that the NV^- centers can be distributed over extended fiber length and uniformly exposed to the magnetic field. Optical fibers enable thus convenient means of the spatial organization of nanodiamonds for efficient coupling of NV fluorescence photons to the fiber guided modes. Localization of

#458162 https://doi.org/10.1364/OE.458162
Journal © 2022 Received 13 Mar 2022; accepted 28 Apr 2022; published 18 May 2022

Optics EXPRESS

diamond particles inside a solid fiber core enables fixation of their positions inside the fiber and provides their mechanical and environmental stability. An important practical advantage of the integration of diamond particles along an optical fiber core is that such fiber probes enable recording of the magnetic response simultaneously from a surrounding limited by the length of the fiber probe itself that can exceed dozens of cm. Moreover, the uniform distribution enhances the read-out contrast (defined as the relative change of the fluorescence intensity at resonance) by reducing the fluorescence of NV^- centers optically excited but not subjected to the magnetic field [15]. These applications have been demonstrated with fibers functionalized with NV^- nanodiamonds either at the fiber-tip [2,5,11] or a tapered section [3,12,13]. In addition to NVs, other color centers in diamond, e.g. germanium-vacancy centers [22] have also been exploited in fiber-tip type sensors for temperature mapping.

However, the introduction of nanodiamonds into the bulk of the fiber core involves drawing of nanodiamond-functionalized glass preforms, which implies severe temperature processing limits and narrows the selection range of relevant fiber glasses.

So far, the integration of nanodiamonds with silica was applied to functionalization of fiber tapers or tips and to the chemical vapor deposition growth of diamond on the fiber end-faces [2]. Bulk doping of diamond particles in the optical fiber core has been realized in tellurite glass fibers and silicate glass fibers [14,15], both of which can be drawn at several hundred degrees centigrade, which is still nondestructive for diamonds. Nanodiamonds in the hollow channels of air-lattice photonic crystal fibers or photonic bandgap air-core fibers have also been demonstrated but results of magnetic field sensing with such fibers have not been reported [16,17].

The coupling of NV^- fluorescence to the guided mode of a fiber may also help to ameliorate the long-standing problem of low photon-collection efficiency of NV^- magnetic field probes. For example, fluorescence from a single NV^- defect in diamond has been coupled to the guided mode of a single mode fiber from a diamond waveguide fixed directly on the fiber taper with van der Waals forces, enabling up to 37% collection efficiency [23]. In volumetric functionalization of fibers with nanodiamonds, enhancement of this efficiency has recently been investigated theoretically through shaping of the fiber structure and layout of nanodiamond particles in the core [18]. Physical realizations involved fibers with diamond particles doped randomly to a tellurite melt drawn into fibers or silicate glass rods, dip-coated with micron-sized particles, and drawn into fibers with the core area delimited by diamonds arranged into a ring [14,15]. The achieved ODMR readout contrast was 3.5% and 2.5%, respectively, while the diamond localization around the core of the latter fiber design reduced the propagation loss down to around 4 dB/m. Nanodiamond functionalization of silica fibers alongside the entire core through the particle deposition from a solvent suspension in cases of the hollow channels, air cores, and suspended glasscore fibers has also been performed [17].

More recently, we have demonstrated the feasibility of controlling diamond particle layout in a transverse plane of the core by multiple stacking of hundreds of glass canes drawn from a single silicate glass rod dip-coated with sub-micron-sized diamond particles [19]. The average diamond-to-diamond separation in the transverse plane of the core was about 1.5 µm, corresponding to the final diameter of the stacked canes constituting the core in the drawn fiber. The achieved ODMR contrast was just over 1% when the NV^- fluorescence was collected from the fiber output as the guided mode and over 5% when collected at the fiber side as its leaky modes.

In this paper, we present the approach to draw a magnetically sensitive optical fiber in which the diamond particles are localized centrally along with a suspended glass core of a diameter not exceeding twice the particle size. Specifically, the achieved fiber core diameter is roughly 1.5 µm against the mean fraction of nanodiamond particles of 750 nm. The proof-of-concept ODMR implementation involved a 24 cm-long section of the developed fiber subjected to a microwave (MW) field created by a loop gap antenna structure, which resulted in almost 7% readout contrast. The fiber showed excellent confinement of the NV^- fluorescence in the guided mode which was

Optics EXPRESS

confirmed by imaging of the excited fiber's side section under a confocal microscope, where hardly any fluorescence and ODMR contrast could be recorded.

2. Fiber probe development

The choice of glasses that can be used for the fabrication of fibers with embedded nanodiamonds is severely limited by the temperature of oxidation (600 °C) and graphitization of diamond particles. In the case described in this paper, two low-melting-point soft silicate glasses were used. An F2 lead silicate glass made by Schott was selected as the glass used for the nanodiamond-functionalized fiber core. Its low transition temperature $Tg_1 = 434$ °C, allows the drawing process to be conducted in temperatures not exceeding 800 °C, which is low enough to limit graphitization of nanodiamonds if nitrogen atmosphere is used. The F2 glass has a refractive index $n_1 = 1.6199$ at the wavelength of 589.3 nm. For the rest of the fiber bulk, a modified-composition F2-like glass was melted in-house with the refractive index $n_2 = 1.6133$ at the wavelength of 589.3 nm and $Tg_2 = 445$ °C [19].

The fiber development process consisted of two stages. The first one was the preparation of the preform components, which included preparation of the F2 glass tube for dip-coating with nanodiamonds. The F2 glass tube used for dip-coating had an external diameter $d_{c1} = 3.4$ mm and internal diameter of $d_{c2} = 2.4$ mm. The suspension liquid was ethanol and the diamond particle concentration was 0.05%. The diamond particles used had a mean diameter of around 750 nm (MDNV1um, Adámas Nanotechnologies), similar to our previous work [19]. The suspension was introduced inside the glass tube and allowed to dry. This process was repeated 10 times, each time with careful avoiding wetting of the tube outside, to ensure even coating of nanodiamonds only at the inside surface of the glass tube. After the final dip-coating, the glass tube was immediately drawn down to a diameter of $d_c = 0.3$ mm. As with all subsequent drawings, at first, the glass tube was heated to a temperature of 400 °C in the oxygen atmosphere to remove any remaining dust particles. Then the fiber drawing was conducted in a temperature range of 710–760 °C, and in the nitrogen atmosphere to reduce graphitization of diamond particles.

In the second stage of the fiber development, the glass preform was assembled and drawn into the final fiber. The first step of the preform assembly procedure consisted of selecting a glass tube with an internal diameter $d_{e1} = 16$ mm and three glass capillaries with an external diameter $d_{t2} = 7.4$ mm. The capillaries were then placed inside the glass tube forming a triangular shape. Free spaces between the glass tube and capillaries were filled with rods made of the same low refractive index glass. Lastly, the previously drawn core capillary with nanodiamonds fused at the inner surface was inserted in the space among the three capillaries. Next, the preform was drawn using a standard drawing tower to form a sub-preform with an outer diameter $d_s = 3.7$ mm. The sub-preform had a fully integrated structure with three holes surrounding a solid glass fiber core. During this process, the core capillary was collapsed, ensuring that the nanodiamonds were placed exactly at the center of the fiber core, which was important to reduce the risk of nanodiamonds protruding beyond the core. Such placement of the diamond particles ensured that during the drawing the nanodiamonds remained in the exact center of the fiber while the pressure necessary to prevent clogging of three side-holes in the fiber structure was equalized. This minimized the risk of structure deformation when drawing the final fiber from the sub-preform. To achieve the suspended core structure with large holes and thin glass bridges, equal pressure was applied to the three holes in the sub-preform microstructure. The final fiber diameter was close to 125 µm. As shown in Fig. 1(a), the thickness of the bridges was approximately 150 - 280 nm, while the core diameter was about 1.5 µm.

Optics EXPRESS

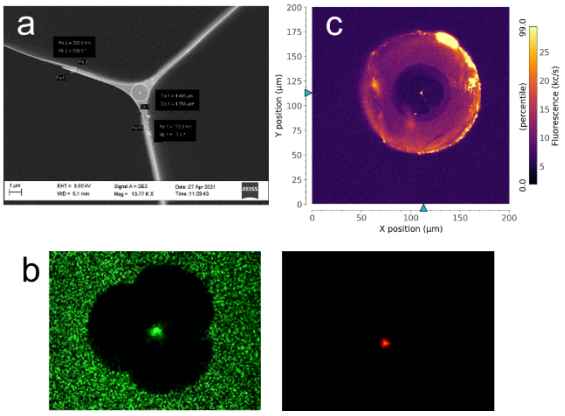

Fig. 1. a) SEM image of the suspended core of the final drawn fiber; b) Standard camera images of the front of the fiber under 532 nm excitation on a white paper background and the same image filtered with a red high-pass filter (FEL0600, Thorlabs); c) Image of the front face recorded with the scanned confocal microscope demonstrating bright NV^- fluorescence inside the fiber.

3. Fiber probe characterization

Basic characterization of the optical properties of the fiber included measurements of the attenuation and bend-loss and imaging of the nanodiamond fluorescence. The attenuation was measured using the cut-back method over five consecutive cuts, from 44 cm, down to 17 cm. The measured fiber loss in the wavelength range of 550-750 nm was 22 dB/m. That high loss value is assigned to the scattering from diamond particles due to a large mismatch between the core glass and diamond refractive indices. Due to the strong mode confinement inherent to the suspended core geometry, the fiber was rather insensitive to bending. The bending losses were measured for very small bending diameters between 65 mm and 15 mm, at a level of 0.2 dB/loop and 0.7 dB/loop respectively. Note that due to a tight bending applied in the measurement, these bending losses reached high values of 14 dB/m and 160 dB/m, respectively. The mode field of the NV^- fluorescence was imaged using a standard camera under the 532 nm continuous wave laser pumping. The fiber output images recorded without and with filtering out of the pump laser light, are shown in Fig. 1(b). Finally, the fiber output facet was imaged by a commercial confocal microscope (Zeiss LSM710) using ten different samples taken evenly from about a 1 m-long section of the fiber. A representative example of the obtained images is shown in Fig. 1(c) and confirms the guiding of the NV^- fluorescence in all investigated samples.

4. Magnetic field sensing performance of the fiber probe

4.1. Experimental setup description

Having characterized the fiber itself, we investigated its magnetic sensitivity by measuring the dependence of optically detected magnetic resonance (ODMR) on the magnetic field. The experimental setup is shown in Fig. 2. The optical readout of the fiber was realized under excitation by the 532 nm continuous-wave laser (Sprout-G, Lighthouse Photonics Inc.). The green light was coupled into the fiber with a microscope objective (Motic 40X, NA=0.65). The NV^- light was collected from the far end of the fiber with a microscope objective (Olympus 40×, NA = 0.75), the 532 nm pump laser background was filtered out using a 600 nm high-pass filter (FEL0600, Thorlabs), and the NV^- fluorescence was detected with a Si avalanche photodetector (APD130A, Thorlabs). This setup allowed effective fluorescence detection over a wavelength

Optics EXPRESS

range of 600–800 nm. To observe the ODMR spectra, a microwave (MW) oscillating field at the frequency around 2.87 GHz was generated using a signal generator (SRS, SG386) and a high-power amplifier (Mini-Circuits ZHL-16W-43+) connected to a loop-gap type inductor ("antenna") structure on a printed circuit board [4]. One fiber end was passed through the opening in the center of the antenna loop which allowed the interaction of this fiber section with the MW field. The fluorescence and ODMR signals were then recorded using an oscilloscope, while the optical fluorescence spectra of the investigated NV$^-$ fiber samples were recorded using a compact grating spectrometer (AvaSpec-3648-USB2, Avantes).

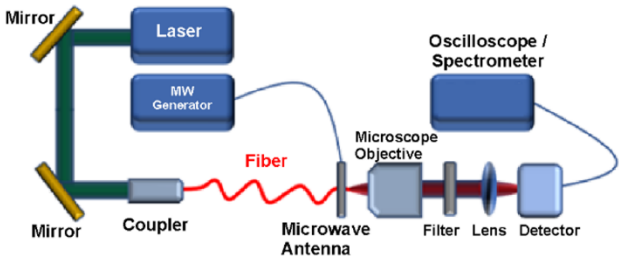

Fig. 2. Experimental setup for magnetic sensing experiments with the developed fiber.

Additionally, the NV$^-$ signals were studied in geometry where the excitation and detection was carried out from the side of the fiber using a home-built wide-field microscopy set-up with the MW field delivered through a microstrip-line positioned along with the fiber. The sample was excited using the 530 nm LED (M530L4, Thorlabs) with optical power around 70 mW passing through a microscope objective (Olympus 40×, NA=0.60) and illuminating the fiber side. The emitted red fluorescence light was collected with the same objective, spectrally filtered by the dichroic mirror and a long-pass filter, and recorded with a CMOS camera (UI-3240CP-NIR, IDS).

4.2. Optical spectra and ODMR signals

We begin with the discussion of the ODMR signal collection with the fiber operated in the transmission mode. The fiber is pumped with the 532 nm laser at one end, and the NV$^-$ fluorescence is collected from the far end of the fiber probe. The optical spectra recorded in this experimental configuration are shown in Fig. 3.

The black trace depicts the spectrum collected from the optical fiber with NV$^-$ color center nanodiamonds. When compared with the reference spectrum from the diamond powder used in the development of the fiber probe represented by a red trace, the black NV-doped spectrum exhibits a noticeable fading of its amplitude at longer wavelengths. The recorded signals were normalized to the intensity at the zero-phonon-line (637 nm) marked with a vertical line. The inset in Fig. 3 shows a weak background signal (magnified here 1000×) observable in a suspended core fiber with identical geometry but without any nanodiamonds.

We attribute that signal to Raman scattering of the 532 nm pump laser. Comparing fluorescence spectra of the nanodiamond functionalized fiber and the standard one with the suspended core, as well as their relative amplitudes, we observe that the Raman scattering in the developed fiber probes does not deteriorate their NV$^-$ fluorescence-related magnetic sensing functionalities. This is in agreement with the earlier observations with the silica glass and the solid-core photonic crystal fibers with nanodiamonds introduced along the core into the fiber's hollow channels [16,17].

The sensitivity of the NV$^-$ diamond-based sensors is mainly determined by the total detected photon flux and the ODMR contrast. To characterize the sensing properties of the developed fiber, we have recorded the continuous-wave ODMR spectra for several values of the magnetic field

Optics EXPRESS

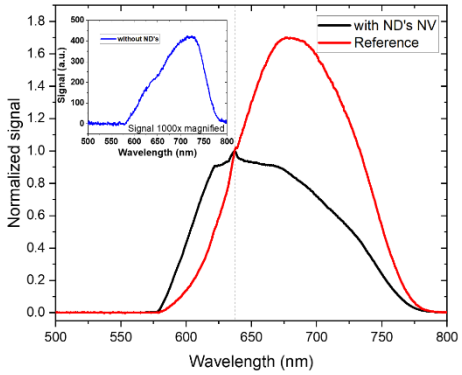

Fig. 3. The optical spectrum of NV⁻ in the developed fiber probe (black trace) against a reference spectrum of NV⁻ nanodiamond powder used for functionalization of the fiber. The inset shows a weak background signal recorded in a reference fiber developed without nanodiamond integration in the suspended core.

intensities (Fig. 4). In zero magnetic field, the ODMR spectrum is similar to those obtained with bulk diamonds. In non-zero fields, however, the spectra are strongly inhomogeneously broadened due to random orientations of individual nanodiamond crystals with respect to the magnetic field direction [4]. Although the orientational inhomogeneity does not permit characterization of the magnetic field direction, the ODMR measurements with nanodiamond-doped fibers enable accurate scalar measurements of the field intensity. This is possible because the outer edges of the resonance correspond to the diamonds with NV⁻ color centers oriented exactly along the direction of the magnetic field, i.e., those exhibiting the maximum field projection on the NV⁻ axis. The accuracy of such measurement can be improved by measuring the frequency-differentiated spectra [4].

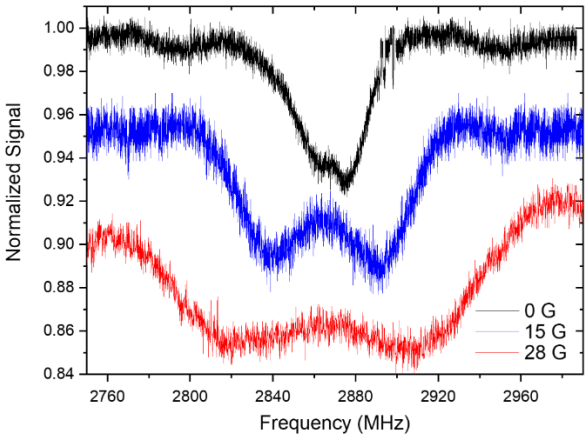

Fig. 4. The ODMR spectra collected from the fiber with excitation and detection from opposite ends of the fiber. Spectra in the non-zero magnetic fields have been vertically offset for clarity.

The ODMR signal contrast achieved with the pump and the NV⁻ fluorescence coupled and collected respectively at the opposite ends of the fiber was almost 7%. The corresponding magnetic field sensitivity can be estimated using the signal slope and the integrated photon flux. For the analyzed suspended core fiber, the photon shot-noise-limited magnetic sensitivity is

Optics EXPRESS

approximately 0.5 $\mu T/\sqrt{Hz}$ at the bias field of B = 1.5 mT. We note that this performance was achieved despite considerable attenuation of the fiber and in a "transmission mode", i.e. in the "end-end" configuration, and leaves much room for improvements. The obtained sensitivity is comparable to the 0.65 $\mu T/\sqrt{Hz}$ value reported by the authors of Ref. [15] who used a nanodiamond ring-core fiber with the side-pumping/collection geometry which reduced to 3 $\mu T/\sqrt{Hz}$ for a 50 cm-long fiber in the longitudinal arrangement. Due to large losses of our fiber probe, the sample length used in our experiments was roughly two times shorter than in Ref. [15]. Magnetic field sensitivity of 0.5 $\mu T/\sqrt{Hz}$ evaluated for the fiber developed in this work is about two orders of magnitude higher than the nanodiamond-on-fiber taper and nanodiamond-on-fiber tip devices reported earlier [3,5,12], although recent optimized devices of that kind reach sub-nT sensitivities [8–10] in very small volumes.

Since no NV^- fluorescence was visible from the side of our suspended-core fiber with wide-field imaging, we filled its side capillaries with immersion oil (refractive index n = 1.518). Still, no diamond particles were directly visible and hardly any fluorescence could be recorded by the camera. Only after integrating the fluorescence from the area highlighted in Fig. 5(a), recording a very weak ODMR signature in zero magnetic field became possible, as shown in Fig. 5(b).

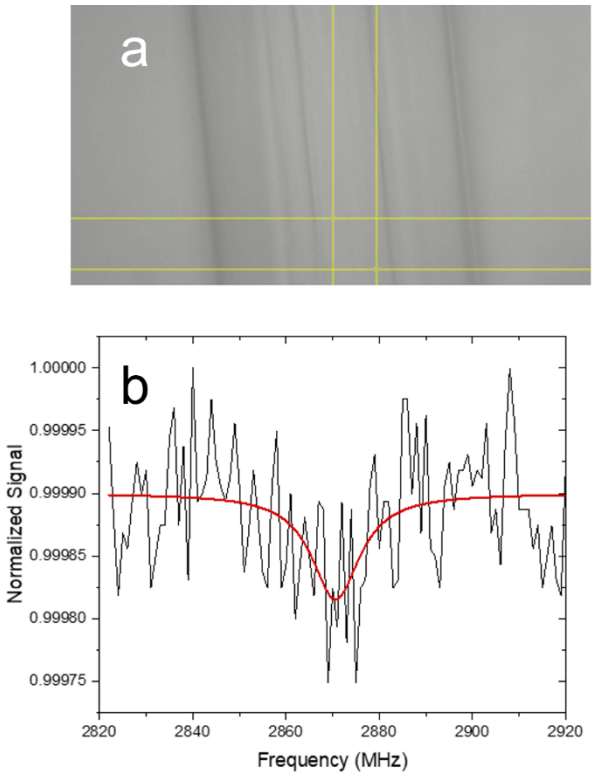

Fig. 5. Probing the fiber from the side in a wide-field microscope: (a) fluorescence image showing no individual nanodiamonds. The same nanodiamonds in the powder form saturate the camera under identical conditions; (b) The ODMR spectrum acquired by integrating light from the area marked in (a). Low contrast results from a large background.

We find the described asymmetry between the amplitudes of the side and longitudinal emissions consistent with the expected enhanced coupling of the fluorescence light into the guided mode. It severely hinders the side observation of the fluorescence and ODMR signals, particularly in the presence of a stray light background and/or camera noise. Admittedly, the described observations

Optics EXPRESS

cannot be treated as exhaustive evidence that the NV^- fluorescence is coupled to the guided mode of the fiber. However, it can indirectly support the hypothesis, that the suspended core fiber geometry with nanodiamonds positioned such that they geometrically overlap most of the guided mode field, facilitates strong NV^- light coupling to the fiber's guided mode.

5. Conclusions

We have demonstrated the fabrication feasibility and proof-of-concept magnetic field sensing application of a nanodiamond-functionalized microstructured optical fiber. The key advantages of the developed fiber stem from its transverse geometry together with the diamond particles being located centrally along the solid glass core suspended on three thin struts. Nanodiamond functionalization of the developed fiber probe exploited a modified dip-coating procedure of the glass tube/preform, in which the diamonds were deposited from a solvent suspension at the inside surface of a glass tube. The joint action of the fiber drawing and collapsing of the tube enabled producing a solid core doped with nanodiamonds, with the ratio of the core diameter to the nano-particle size of 2:1. In that way, we successfully combined the fiber's strong optical confinement within the direct overlap of the nanodiamond particles with the guided mode. While a strict description of the NV^- fluorescence coupling efficiency to the guided mode of the fiber would require additional experiments and modelling, which was outside of the scope of the current work, the presented results illustrate the magnetic sensing performance of the developed fiber. The magnetic field sensitivity of 0.5 $\mu T/\sqrt{Hz}$ was achieved with the readout from the fiber's guided mode, and exceeds earlier reports by roughly two orders of magnitude, providing a supportive proof-of-concept of the suspended core fiber configuration for NV^- based sensors.

These preliminary results leave room for further improvements. In particular, we expect that using smaller nanodiamonds would improve the sensor's performance by better homogeneity within the fiber and lowering the scattering losses. The sensor's sensitivity, would definitely benefit from application of pulse techniques, like spin-echo and/or dynamic decoupling. Future applications of the efficiently guiding probes could be, e.g., for the magnetic-field-gradient sensors (gradiometers) with multiple fibers. Moreover, the air channels, intrinsic to the concept of the suspended core fibers, make it possible to realize various microfluidic sensing implementations. Our current demonstration uses a lead silicate glass, which, admittedly, is not as sturdy as silica and is incompatible with fusion splicing with silica fibers. However, the F2 glass is mechanically robust, crystallization resistant and, when compared to silica, can be drawn into fibers using standard fiber drawing equipment. The low-cost parameter of F2-based fibers is important for bio-sensor applications because it facilitates their commissioning as single-use devices, which becomes increasingly popular for many bio-diagnostic components.

Funding. Fundacja na rzecz Nauki Polskiej (TEAM NET POIR.04.04.00-00-1644/18).

Disclosures. The authors declare no conflicts of interest.

Data Availability. Data underlying the results presented in this paper are not publicly available at this time but may be obtained from the authors upon reasonable request.

References

1. F. Jelezko, T. Gaebel, I. Popa, A. Gruber, and J. Wrachtrup, "Observation of Coherent Oscillations in a Single Electron Spin," Phys. Rev. Lett. **92**(7), 076401 (2004).
2. J. R. Rabeau, S. T. Huntington, A. D. Greentree, and S. Prawer, "Diamond chemical-vapor deposition on optical fibers for fluorescence waveguiding," Appl. Phys. Lett. **86**(13), 134104 (2005).
3. I. V. Fedotov, L. V. Doronina-Amitonova, D. A. Sidorov-Biryukov, N. A. Safronov, A. O. Levchenko, S. A. Zibrov, S. Blakley, H. Perez, A. V. Akimov, A. B. Fedotov, P. Hemmer, K. Sakoda, V. L. Velichansky, M. O. Scully, and A. M. Zheltikov, "Fiber-optic magnetometry with randomly oriented spins," Opt. Lett. **39**(23), 6755–6758 (2014).
4. A. M. Wojciechowski, P. Nakonieczna, M. Mrózek, K. Sycz, A. Kruk, M. Ficek, M. Głowacki, R. Bogdanowicz, and W. Gawlik, "Optical Magnetometry Based on Nanodiamonds with Nitrogen-Vacancy Color Centers," Materials **12**(18), 2951 (2019).

Optics EXPRESS

5. I. V. Fedotov, L. V. Doronina-Amitonova, D. A. Sidorov-Biryukov, N. A. Safronov, S. Blakley, A. O. Levchenko, S. A. Zibrov, A. B. Fedotov, S. Ya. Kilin, M. O. Scully, V. L. Velichansky, and A. M. Zheltikov, "Fiber-optic magnetic-field imaging," Opt. Lett. **39**(24), 6954–6957 (2014).
6. I.V. Fedotov, L.V. Doronina-Amitonova, A.A. Voronin, A.O. Levchenko, S.A. Zibrov, D.A. Sidorov-Biryukov, A.B. Fedotov, V.L. Velichansky, and A.M. Zheltikov, "Electron spin manipulation and readout through an optical fiber," Sci. Rep. **4**(1), 5362 (2014).
7. A. K. Dmitriev and A. K. Vershovskii, "Concept of a microscale vector magnetic field sensor based on nitrogen-vacancy centers in diamond," J. Opt. Soc. Am. **33**(3), B1–B4 (2016).
8. R.L. Patel, L.Q. Zhou, A.C. Frangeskou, G.A. Stimpson, B.G. Breeze, A. Nikitin, M.W. Dale, E.C. Nichols, W. Thornley, B.L. Green, M.E. Newton, A.M. Edmonds, M.L. Markham, D.J. Twitchen, and G.W. Morley, "Subnanotesla Magnetometry with a Fiber-Coupled Diamond Sensor," Phys. Rev. Appl. **14**(4), 044058 (2020).
9. F. M. Stürner, A. Brenneis, T. Buck, J. Kassel, R. Rölver, T. Fuchs, A. Savitsky, D. Suter, J. Grimmel, S. Hengesbach, M. Förtsch, K. Nakamura, H. Sumiya, S. Onoda, J. Isoya, and F. Jelezko, "Integrated and Portable Magnetometer Based on Nitrogen-Vacancy Ensembles in Diamond," Adv. Quantum Technol. **4**, 2000111 (2021).
10. G. Chatzidrosos, J. S. Rebeirro, H. Zheng, M. Omar, A. Brenneis, F. M. Stürner, T. Fuchs, T. Buck, R. Rölver, T Schneemann, P. Blümler, D. Budker, and A. Wickenbrock, "Fiberized Diamond-Based Vector Magnetometers," Front. Photon. **2**, 732748 (2021).
11. T. Schröder, A. W. Schell, G. Kewes, T. Aichele, and O. Benson, "Fiber-Integrated Diamond-Based Single Photon Source," Nano Lett. **11**(1), 198–202 (2011).
12. X. Liu, J. Cui, F. Sun, X. Song, F. Feng, J. Wang, W. Zhu, L. Lou, and G. Wang, "Fiber-integrated diamond-based magnetometer," Appl. Phys. Lett. **103**(14), 143105 (2013).
13. M. Fujiwara, O. Neitzke, T Schröder, A. W. Schell, J. Wolters, J. Zheng, S. Mouradian, M. Almoktar, S. Takeuchi, D. Englund, and Oliver Benson, "Fiber-Coupled Diamond Micro-Waveguides toward an Efficient Quantum Interface for Spin Defect Centers," ACS Omega **2**(10), 7194–7202 (2017).
14. Y. Ruan, H. Ji, B. C. Johnson, T. Ohshima, A. D. Greentree, B. C. Gibson, T. M. Monro, and H. Ebendorff-Heidepriem, "Nanodiamond in tellurite glass Part II: practical nanodiamond-doped fibers," Opt. Mater. Express **5**(1), 73–87 (2015).
15. D. Bai, M. H. Huynh, D. A. Simpson, P. Reineck, S. A. Vahid, A. D. Greentree, S. Foster, H. Ebendorff-Heidepriem, and B. C. Gibson, "Fluorescent diamond microparticle doped glass fiber for magnetic field sensing," APL Mater. **8**(8), 081102 (2020).
16. I. V. Fedotov, N. A. Safronov, Yu. A. Shandarov, A. Yu. Tashchilina, A. B. Fedotov, A. P. Nizovtsev, D. I. Pustakhod, V. N. Chizevski, T. V. Matveeva, K. Sakoda, S. Ya. Kilin, and A.M. Zheltikov, "Photonic-crystal-fiber-coupled photoluminescence interrogation of nitrogen vacancies in diamond nanoparticles," Laser Phys. Lett. **9**, 151 (2011).
17. I. V. Fedotov, N. A. Safronov, Yu. A. Shandarov, A. A. Lanin, A. B. Fedotov, S. Ya. Kilin, K. Sakoda, M. O. Scully, and A. M. Zheltikov, "Guided-wave-coupled nitrogen vacancies in nanodiamond-doped photonic-crystal fibers," Appl. Phys. Lett. **101**(3), 031106 (2012).
18. S. Li, D. Bai, M. Capelli, Q. Sun, and S. Afshar V., D. A. Simpson, S. Foster, H. Ebendorff-Heidepriem, B. C. Gibson, and A. D. Greentree, "Preferential coupling of diamond NV centres in step-index fibres," Opt. Express **29**(10), 14425–14437 (2021).
19. A. Filipkowski, M. Mrózek, G. Stępniewski, J. Kierdaszuk, A. Drabińska, T. Karpate, M. Głowacki, M. Ficek, W. Gawlik, R. Buczyński, A. Wojciechowski, R. Bogdanowicz, and M. Klimczak, "Volumetric incorporation of NV diamond emitters in nanostructured F2 glass magneto-optical fiber probes," Carbon **196**, 10–19 (2022).
20. Shai Maayani, Christopher Foy, Dirk R. Englund, and Yoel Fink, "Distributed Quantum Fiber Magnetometry," Laser Photonics Rev. **13**, 1900075 (2019).
21. A. Beveratos, R. Brouri, T. Gacoin, J.-P. Poizat, and P. Grangier, "Nonclassical radiation from diamond nanocrystals," Phys. Rev. A **64**(6), 061802 (2001).
22. S. M. Blakley, C. Vincent, I. V. Fedotov, X. Liu, K. Sower, D. Nodurft, J. Liu, X. Liu, V. N. Agafonov, V. A. Davydov, A. V. Akimov, and A. M. Zheltikov, "Photonic-Crystal-Fiber Quantum Probes for High-Resolution Thermal Imaging," Phys. Rev. Appl. **13**(4), 044048 (2020).
23. R. N. Patel, T. Schröder, N. Wan, L. Li, S. L. Mouradian, E. H. Chen, and D. R. Englund, "Efficient photon coupling from a diamond nitrogen vacancy center by integration with silica fiber," Light: Sci. Appl. 5(2), e16032 (2016).